Supplementary Figures

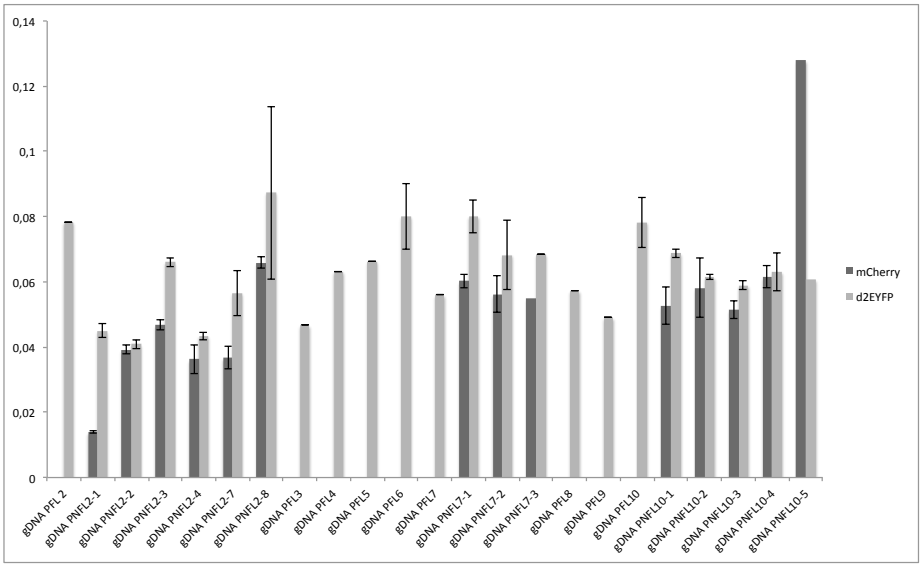

Supplementary Figure S1: **d2EYFP and mCherry integration levels in PFL and PNFL clonal cell populations.** Real-time PCR was performed on genomic DNA extraction from CHO cells to compare the rate of viral integration of each motif in monoclonal populations. Error bars represent the standard error among three replicates.

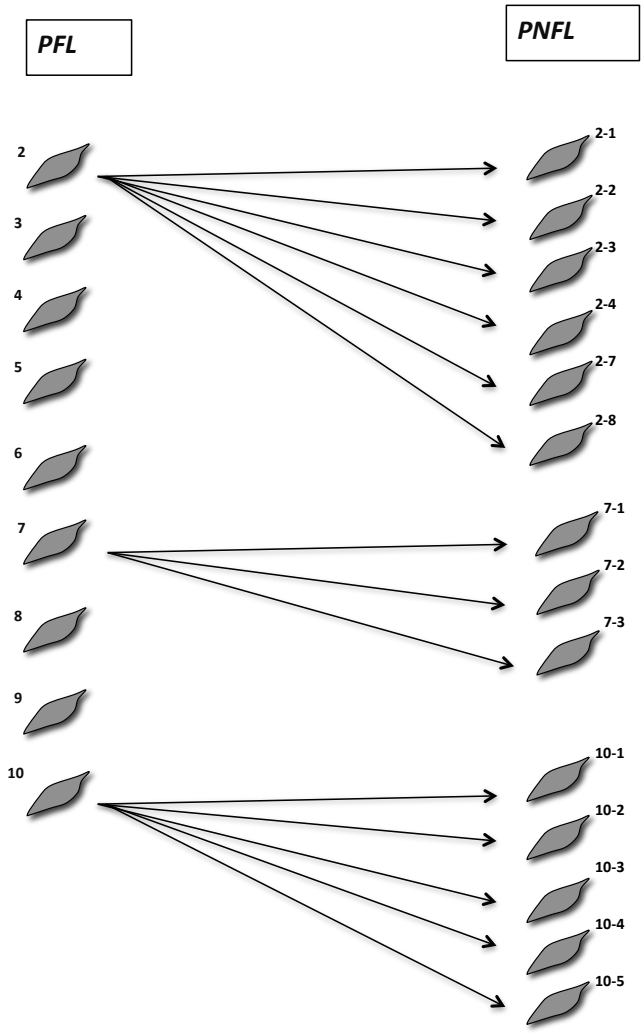

Supplementary Figure S2: **Clone Tree.** PFL clones were derived from the first Lentiviral infection of CHO wild type cells while PNFL clones were derived from the second Lentiviral infection performed on sorted monoclonal populations of PFL cells.

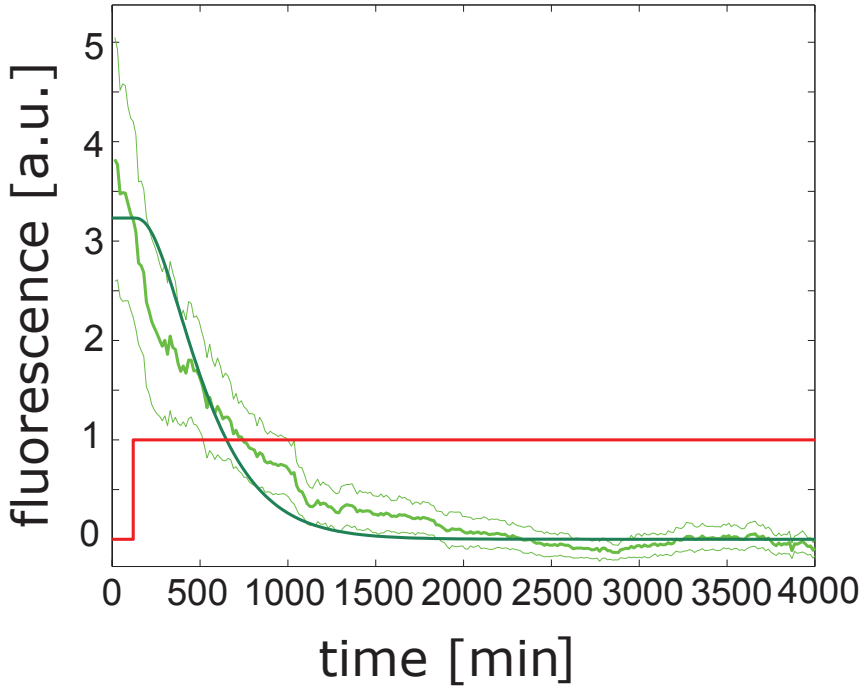

Supplementary Figure S3: **Fitting of the PNFL parameters.** A switch off experiment was performed to estimate the unknown parameters of the PNFL model. The red line represents Doxycycline treatment; the solid bright green line represents the mean fluorescence measured on 23 replicates; the thin lines represents standard deviation, while the dark green line represents the best fit obtained with the PNFL model.

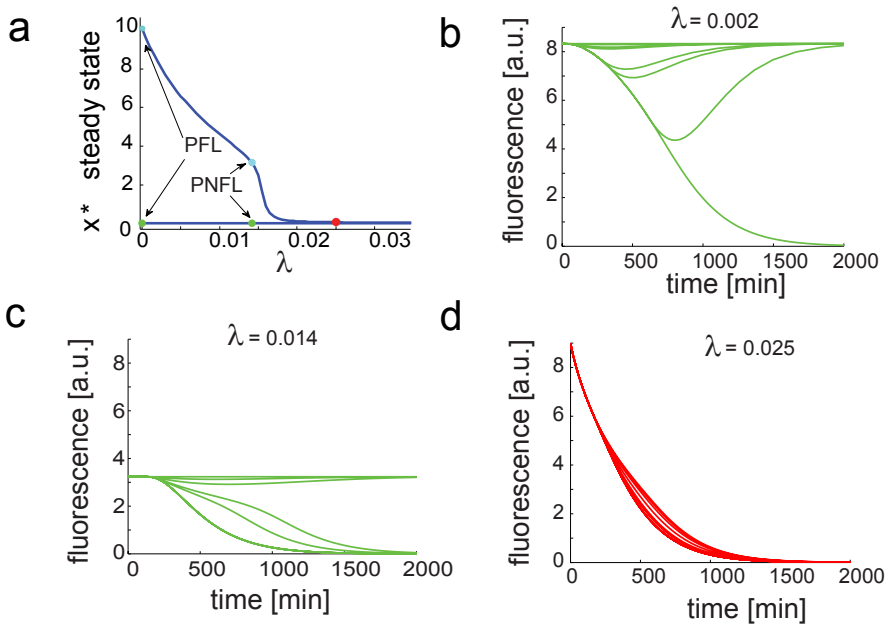

Supplementary Figure S4: **Bifurcation diagram and simulated "switch off" time-course across the PNFL cell population following different pulses of Doxycycline and with different miRNA strengths (λ). (a)** Bifurcation diagram of PNFL model with respect to the parameter λ. When $\lambda = 0$ ($\lambda = 0.014$), the model represents the PFL (PNFL); in both cases the systems are bistable (green dot = OFF state, cyan dot = ON state). For high values of λ, the system is no more bistable and the two equilibria collapse (red point). **(b)** - **(c)** Different switch off time-courses were simulated by varying the parameter λ representing the strength of miRNA mediated degradation of the tTA mRNA; the value of λ can tune the dynamics of the PNFL by making it faster (stronger repression) or slower (weaker repression). (d) The same simulation is proposed for $\lambda = 0.025$ when the system is not bistable.

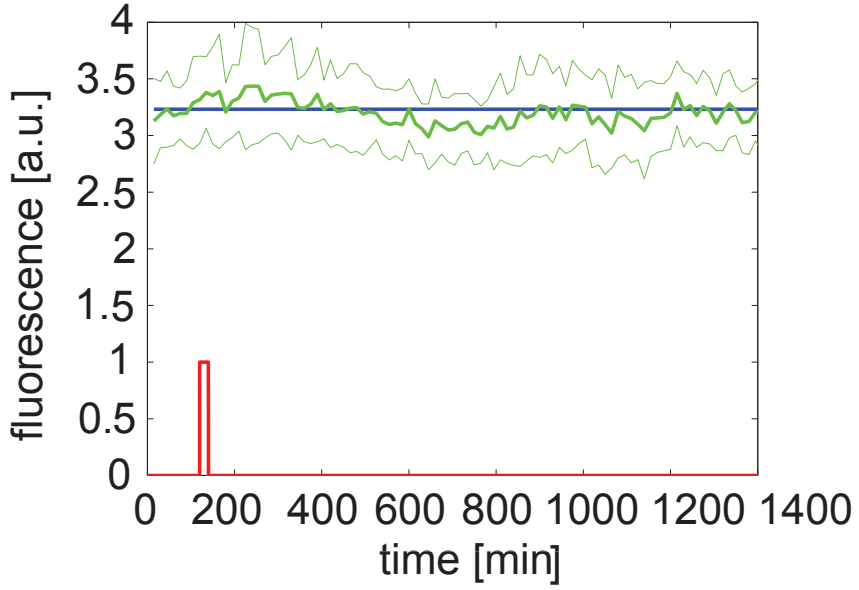

Supplementary Figure S5: **In silico and in vitro "switch OFF" experiment for PNFL cells following a short pulse of Doxycycline.** Simulated (blue line) and experimental (solid green line) d2EYFP fluorescence of PNFL 7-2 cells following a 20 min pulse of Doxycycline. Experimental data were obtained using the microfluidic device. Treatment with Doxycycline (red line) was performed at time 120 min and removed after 20 min. Standard deviation (thin green line) is among six replicates; experimental data are rescaled to simulation values.

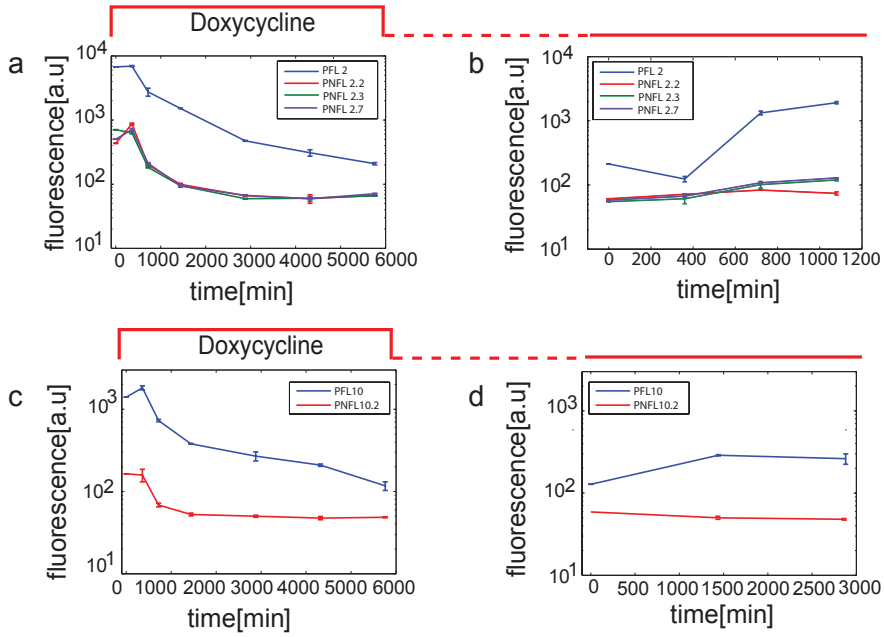

Supplementary Figure S6: **Fluorescence-Activated Cell Sorting (FACS) switch off experiment of PFL 2, PFL 10 cells and the corresponding PNFL cells. (a)**: d2EYFP fluorescence levels in PFL 2 cells (blue line) and PNFL 2-2, 2-3, 2-7 (respectively red, green and purple lines) were measured at 0 hrs, 6 hrs (360 min), 12 hrs (720 min), 24 hrs (1440 min), 48 hrs (2880 min) and 72 hrs (4320 min) following treatment with Doxycycline (1 μg/ml) at time 0 hrs. **(b)**: d2EYFP fluorescence levels in PFL cells (blue line) and PNFL cells (red, green and purple lines) cells were measured at 0, 6, 12, 18 hrs following removal of Doxycycline at time 0 hrs. Prior to time 0 hrs, both PFL and PNFL cells were grown in the presence of Doxycycline for 72 hrs. **(c)**: d2EYFP fluorescence levels in PFL 10 cells (blue line) and PNFL 10-2 (red line) were measured at 0 hrs, 6 hrs (360 min), 12 hrs (720 min), 24 hrs (1440 min), 48 hrs (2880 min) and 72 hrs (4320 min) following treatment with Doxycycline (1 μg/ml) at time 0 hrs. **(d)**: d2EYFP fluorescence levels in PFL cells (blue line) and PNFL cells (red line) cells were measured at 0 hrs, 24 hrs (1440 min), and 48 hrs (2880 min) following removal of Doxycycline at time 0 hrs. Prior to time 0 hrs, both PFL and PNFL cells were grown in the presence of Doxycycline for 72 hrs. Error bars represent the standard deviation among three replicates.

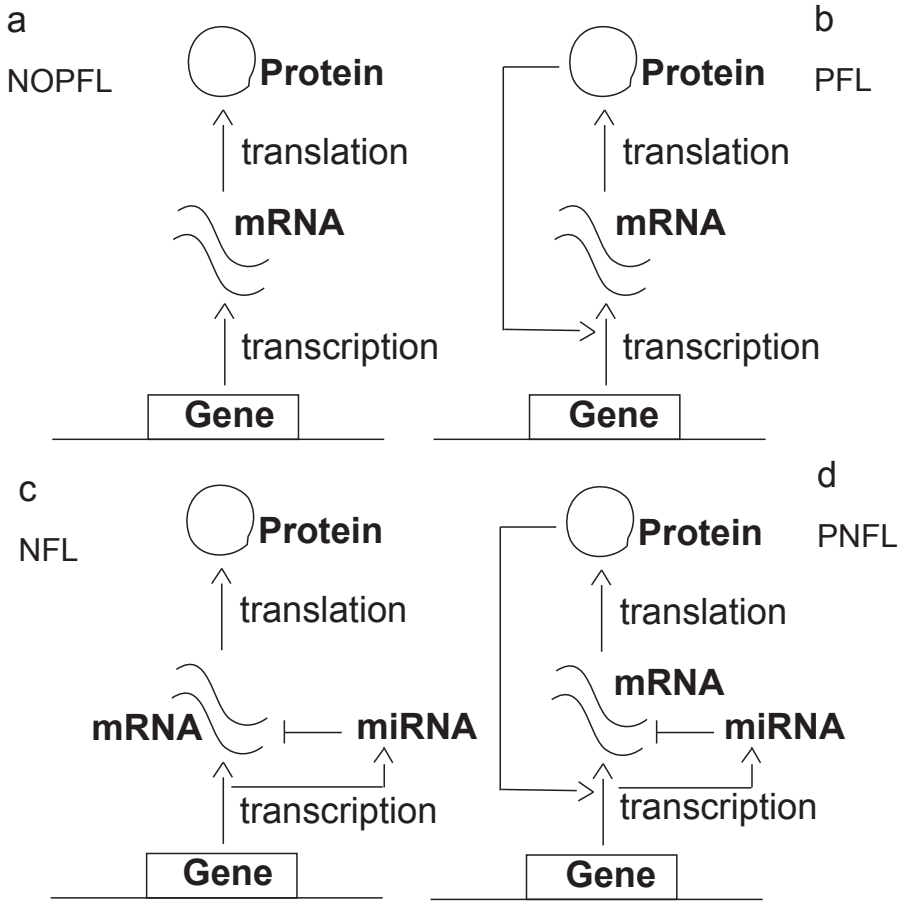

Supplementary Figure S7: **Scheme of NOPFL, PFL, NFL, PNFL circuits. (a)** Open Loop circuit as represented in [34] and corresponding to the NOPFL circuit [24]. (b) PFL where the transcription feedback activates its own transcription. (c) Negative Feedback Loop mediated by a microRNA inducing degradation of the target mRNA. **(d)** A symplified scheme for PNFL system, represented as a combination of PFL and NFL.

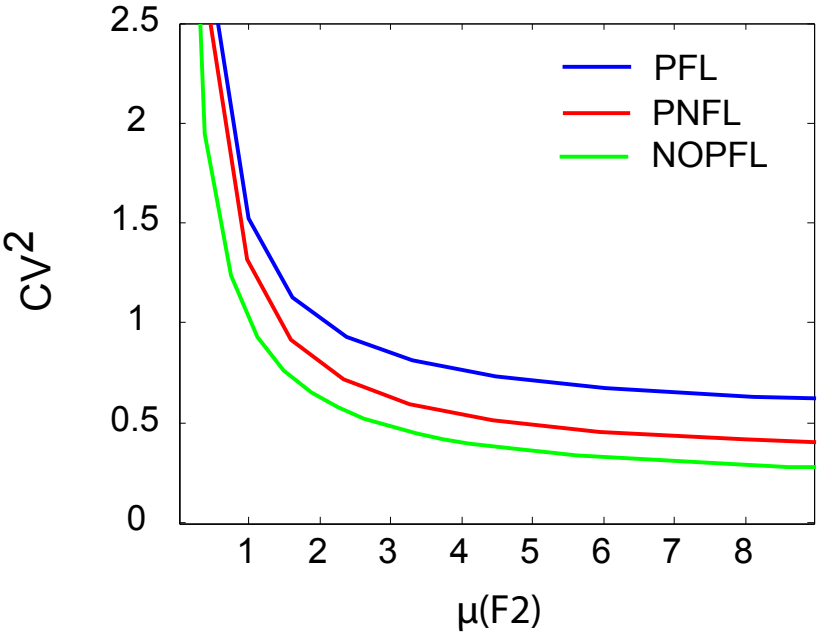

Supplementary Figure S8: CV^2 **as function of the mean fluorescence as derived from the simulation of the Master Equations.** The blue line represents the CV^2 of the PFL while the red line is the CV^2 of the PNFL. The green line is the CV^2 of the NOPFL as previously estimated in [31].

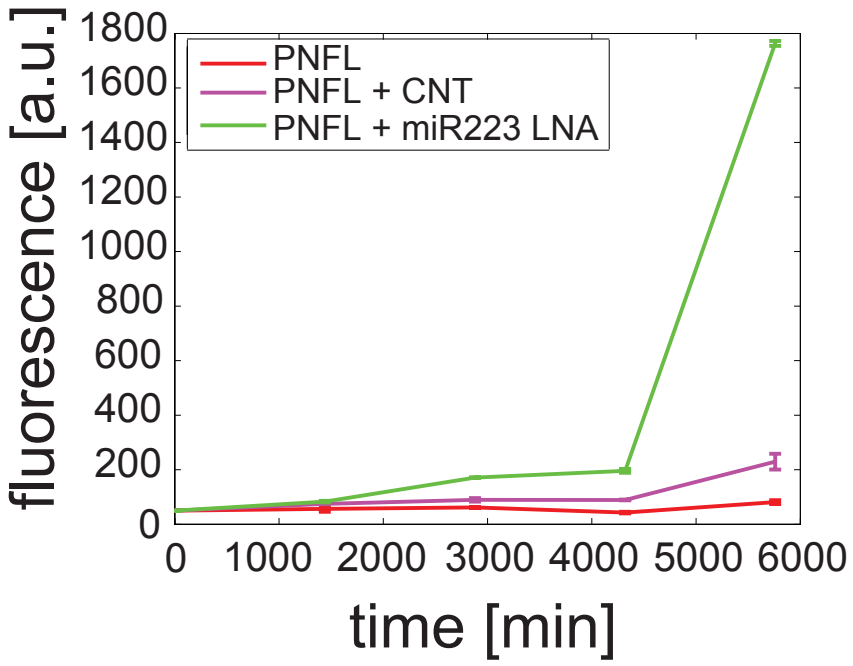

Supplementary Figure S9: **Fluorescence-Activated Cell Sorting (FACS) switch on experiment of PNFL 7-2 cells transfected with Locked Nucleic Acid 223 (LNA 223).** d2EYFP fluorescence level in PNFL cells trasfected with 150 pmol of LNA 223 (green line), LNA negative control (magenta line) and not trasfected (red line) were measured at 0 hrs , 24 hrs (1440 min), 48 hrs (2880 min), 96 hrs (5760 min) following removal of Doxycycline at time 0 hrs. Prior to time 0 hrs, PNFL cells were grown in the presence of Doxycycline for 72 hrs and the cells were trasfected after 24 hrs from Doxycycline removal. Error bars represent the standard deviation among three replicates.

Supplementary Tables

Supplementary Table S1: Parameters for the PFL / PNFL system.

Parameters	Definition	unit	Value
G_1	insertion point for the first construct		1.058
G_2	insertion point for the second construct		0.301
v_1	maximal transcription rate for CMVTET promoter	$[nMmin^{-1}]$	0.075432
v_2	translation rate for tTA protein	$[min^{-1}]$	0.027131449
v_3	maximal transcription rate for CMVTET promoter	$[nMmin^{-1}]$	0.075432026
v_4	translation rate for mCherry	$[min^{-1}]$	0.0271
d_1	degradation rate for tTA mRNA	$[min^{-1}]$	0.01012906
d_2	degradation rate for tTA protein	$[min^{-1}]$	0.010016646
d_3	degradation rate for miR223 mRNA	$[min^{-1}]$	0.0012351
d_4	degradation rate for d2EYFP protein	$[min^{-1}]$	0.00453
d_5	degradation rate for mCherry protein	$[min^{-1}]$	0.00048135
α_1	basal activity for CMVTET promoter		0.000011292
λ	maximal rate of silencing	$[min^{-1}]$	0.0142
K_1	Hill constant for miR223 equation	$[nM]$	4.807645104
K_3	Hill constant for d2EYFP equation	$[nM]$	3.97
K_D	folding rate for miR223	$[nM]$	0.0142
h_1	Hill constant for miR223 equation		3.163
h_3	Hill constant for d2EYFP equation		4

Supplementary Table S2: Parameters for the stochastic model of CV^2 as represented in Figure 7 of the main text.

Parameters	numeric value
$< B >$	0.5595
$< B^2 >$	6.1434
k	0.7508
$\overline{k}$	0.6077

Supplementary Table S3: Parameters for the simulations reported in Figure S8. Note that the common parameters are described by the same values.

Parameters	numeric value
$\overline{K_w}$	1.1882
${K_w}^0$	0.143
${K_w}^1$	0.2331
$\overline{K_r}$	$=\overline{K_w}$
${K_r}^0$	$= {K_w}^0$
${K_r}^1$	$= {K_w}^1$
K_q	1.3621
g_w	0.4847
g_q	0.6557
g_r	0.3
${\beta_w}^0$	0.01
${\beta_w}^1$	0.005

Supplementary Notes

Supplementary Note 1: Construction and integration in Chinese Hamster Ovary (CHO) cells of a synthetic Positive-Negative(PNFL)feedback network

The synthetic circuit was implemented in a lentiviral vector, by using the ViraPower Promoterless Lentiviral Gateway Expression System (Invitrogen).

The pMAtTA-IRES-EGFP-WPRE vector containing the transactivator *tTA*, the IRES element, the enhanced green fluorescent protein (*EGFP*) and the WPRE, was synthesised by GENEART together with the recombination sites. The *d2EYFP* coding sequence was amplified from pd2EGFP-1 (Clontech) by PCR with a forward primer containing a NheI recognition sequence (5'-CATGGC TAGCATGGTGAGCAAGGGCGAGGAG-3') and a reverse primer containing an EcoRV recognition sequence (5'- ATTCGATATCAGTCGCGGCCGCATCT ACA-3'). The PCR product and pMAtTA-IRES-EGFP were then digested with NheI-EcoRV restriction enzymes and the *d2EYFP* ligated in place of *EGFP*, generating a new vector termed pMAtTA-IRES-d2EYFP.

The pMAtTA-IRES-d2EYFP was then linearised with the AseI restriction enzyme and recombined with the pDONR221 (Invitrogen) following the manufacturer instruction. In this way we generated pENTRtTA-IRES-d2EYFP vector with specific recombination sites, as previously described [24].

The pMA-miR223-destRFP-WPRE vector containing the first intron of the low affinity nerve growth factor receptor *(δLNGFR)* with the natural miRNA-223, and the destabilized form of Red Fluorescent Protein *RFP* reporter gene was synthesised by GENEART together with the recombination sites. *mCherry* fluorescent protein coding sequence was amplified from the pmCherry (Clontech) by PCR with a forward primer containing a NheI recognition sequence (5'-CATGGCTAGCATGGTGAGCAAGGGCGAGGAG-3'), and a reverse primer containing a NotI restriction site (5'-ATTCGCGGCCGCTTACTTGTACAGCT CGTCCATGCC-3'). The PCR product and pMA-miR223-destRFP-WPRE were then digested with NheI-NotI restriction enzymes and the mCherry ligated in place of destRFP, generating a new vector termed pMA-miR223-mCherry.

The pMA-miR223-mCherry was then linearised with the AseI restriction enzyme and recombined with the pDONR221 (Invitrogen) following the manufacturer instruction. In this way we generated pENTR-miR223-mCherry vector with specific recombination sites.

The *CMV-TET* promoter was amplified from pTRE2 (Clontech) by PCR. The PCR was performed with the Taq polymerase provided by Invitrogen that adds a single deoxyadenosine (A) to the 3' ends of PCR products. This allows PCR inserts to ligate efficiently with the pENTR5'-TOPO vector which is supplied linearised with single 3'-deoxythymidine (T) overhangs, obtaining the pENTR5'-TOPO-*CMV-TET* with specific recombination sites.

Finally we performed recombination reactions between the pENTRtTA-IRES-d2EYFP/pENTR-miR223-mCherry, pENTR5'-TOPO-*CMV-TET* and the pLenti/R4R2/V5-DEST according to manufacturer instructions. As suggested by the manufacturer, the lentivirus at a MOI=1 (one integration event per cell at the moment of transduction) was produced in 293FTcells.

We infected Chinese Hamster Ovary (CHO) cells with the PFL motif, which were first sorted by Fluorescence Activated Cell Sorter (FACS) and then clonal populations of CHO cells carrying the PFL construct were generated by single cell expansion (PFL cells). In this way we generated nine monoclonal population of PFL-CHO cells. We next infected, and sorted according to expression of Green and Red fluorescence by FACS, PFL-CHO cells with the virus carrying the negative feedback loop, obtaining PNFL-CHO cells. From heterogenous population, we selected fourteen PNFL-CHO clonal population. We compared the number of d2EYFP genomic DNA integration in all the clonal populations by Real-Time PCR S1. (Experimental procedure: DNA extraction, RealTime PCR).

The miR 223 was inserted in the first intron of the low affinity nerve growth factor receptor *(δLNGFR)* such that the miRNA is spliced out, and so the cleavage of pre-miRNA by Drosha does not affect the integrity of the whole mRNA that otherwise would lose the 5′-cap or the poly-A tail thus compromising the protein production [23].

Supplementary Note 2: DNA extraction, RealTime PCR

10^6 PFL and PNFL cells were plated in a 6-well multiwell plate to reach a confluence of 80% for DNA extraction. The day after cells were collected and re-suspended in 200μL of PBS after centrifugation for five minutes at 300 x g . Then the DNA was extracted using the DNeasy Blood and Tissue kit (Qiagen). We compared the DNA levels of *mCherry* and *d2EYFP* in PNFL cells and PFL cells by RealTime PCR following DNA extraction, proving that the both cell populations carry a unique copy of the networks in their genome. Quantitative RealTime PCR reaction were set up in duplicates using the LightCycler 480 SYBR green master mix (Roche) and the amplification was performed using a LightCycler 480 RealTime PCR instrument(Roche). The PCR were carried out using the following primers: d2EYFP forward (5'-ACGACGGCACTCAAGACC-3'); d2EYFP reverse (5'-GTCCTCCTTGAAGTCGATGC-3'); mCherry forward (5'-CACTACGACGCTGAGGTCAAG-3'); mCherry reverse (5'-GTAGTC CTCGTTGTGGGAGGT-3'). Data analyses were performed using the LightCycler 480 Software(Roche). *GAPDH* DNA levels were used to normalise the amount of DNA and ΔCts were calculated as the difference between the average *GAPDH* Ct and the average *mCherry* and *d2EYFP*.

Supplementary Note 3: Dynamic model of the PNFL

In order to study the dynamic behaviour of the PNFL motif to compare it with the one of the PFL motif, we first derived a mathematical model based on ordinary differential equations (ODEs) and then compared it to an ODE model we previously derived for the PFL motif ([24]).

In deriving the models, we made the following assumptions:

- Hill functions to model the rate of gene transcription, including basal activity to describe the leakiness of the $CMV - TET$ promoter;
- linear degradation for all genes and proteins;
- linear dynamics for the translation;

- Hill functions to model the effect of the inducer (Doxycycline);
- Hill functions to consider the effect of the post-transcriptional inhibition of the miRNA on tTA mRNA ([51]);
- distinct dynamics for the inactive and active forms of the miRNA in order to consider the delay in the formation of mature microRNA;
- distinct dynamics for the unfolded (inactive) and folded (active) forms of the reporter proteins (d2EYFP, mCherry), in order to include the protein maturation needed for a correct protein folding ([54]).

Each equation describes a species, i.e. mRNA and the correspondent protein concentration, taking into account the change in concentration of the species in a given time interval, as the result of a production term and a degradation term. The set of ODEs describing the PNFL motif is reported below:

$$\frac{dx_1}{dt} = G_1 v_1 \left(\alpha_1 + (1-\alpha_1) \frac{\left(\frac{\theta^{h_0}}{\theta^{h_0}+D^{h_0}} x_2\right)^{h_2}}{K_1^{h_2} + \left(\frac{\theta^{h_0}}{\theta^{h_0}+D^{h_0}} x_2\right)^{h_2}} \right) - d_1 x_1 - \lambda \frac{{x_4}^{h_3}}{{K_3}^{h_3} + {x_4}^{h_3}} x_1 \tag{S1}$$

$$\frac{dx_2}{dt} = v_2 x_1 - d_2 x_2 \tag{S2}$$

$$\frac{dx_3}{dt} = G_2 v_1 \left(\alpha_1 + (1-\alpha_1) \frac{\left(\frac{\theta^{h_0}}{\theta^{h_0}+D^{h_0}} x_2\right)^{h_2}}{K_1^{h_2} + \left(\frac{\theta^{h_0}}{\theta^{h_0}+D^{h_0}} x_2\right)^{h_2}} \right) - (d_3 + K_D) x_3 \tag{S3}$$

$$\frac{dx_4}{dt} = K_D x_3 - \delta x_4 \tag{S4}$$

$$\frac{dx_5}{dt} = v_4 x_1 - (K_{fg} + d_4) x_5 \tag{S5}$$

$$\frac{dx_6}{dt} = K_{fg} x_5 - d_4 x_6 \tag{S6}$$

$$\frac{dx_7}{dt} = v_3 x_3 - (K_{fr} + d_5) x_7 \tag{S7}$$

$$\frac{dx_8}{dt} = K_{fr} x_7 - d_5 x_8 \tag{S8}$$

where

- x_1 is the tTA mRNA,
- x_2 is the tTA protein,
- x_3 is the miR223 mRNA,
- x_4 is the miR223 mRNA in the active form
- x_5 is the d2EYFP unfolded protein,
- x_6 is the d2EYFP folded protein,
- x_7 is the mCherry unfolded protein,
- x_8 is the mCherry folded protein.

By setting the variable x_3 and x_4 to zero (describing the immature and mature miR223), as well as the variable x_7 and x_8 (describing the mCherry protein) the model for the PNFL motif becomes equal to the model for the PFL motif previously reported [24].

In order to compare the PNFL motif with the PFL motif, we fixed the parameter of the PFL model to the previously determined values [24]; whereas for the PNFL model, all the common parameters with the PFL model (i.e. the production and degradation rate of the tTA and d2EYFP and the Hill functions describing the tTA self-activation and the effect of Doxycycline) have the same values as in the PFL model, while the remaining parameters were chosen to obtain a Least Squared Error fit to the d2EYFP fluorescence time-course when a complete switch off experiment using Doxycyline is performed, as reported in Supplementary Figure S3 and as described later. The list of all the parameters is reported in Supplementary Table S1.

Using numerical bifurcation analysis, we observed that the PNFL motif can exhibit bistabilty, as shown in Supplementary Figure S4a, just like the PFL motif [24].

We then simulated a series of "switch off" experiments for both the PFL and PNFL motifs: the switch off simulations were performed by setting as

initial conditions for solving Eqs. S1-S8, the values of the state variables at the ON steady state, we then simulated pulses of Doxycycline treatment (at a concentration of $1\mu g/ml$) of different durations Δ.

Simulation results are shown in the main text in Figure 1 and Figure 2. Simulation are measured in Model Units (m.u.) and experiments in Arbitrary Units (a.u.). The simulated data were rescaled to the experimental units by using a linear function ($y_{rescaleddata} = ax_{data} + b$). For PFL, the rescaling factors a and b are $(3, -5)$ and $(1.847, 0)$ respectively for $\Delta = 960$ min and $\Delta = 1800$ min; for PNFL, the rescaling factors are $(2.15, 2.82)$ and $(1.92, 1.32)$ respectively for $\Delta = 240$ min and $\Delta = 60$ min.

Numerical simulations were run using Matlab 2010b (Mathworks Inc.). We used *ode*23*s* solver (a detailed discussion of the numerical methods used by *ode*23 can be found in [52]). For the parameter identification, we used the PottersWheel toolbox [50] implemented in MATLAB, as also described in ([24]).

Supplementary Note 4: Microfluidic device fabrication protocol

The microfluidic device described in [49] was produced at the University of California, San Diego and Istituto per la Microelettronica e Microsistemi, Naples. A master mold has been produced using a 4" silicon wafer as substrate (Silicon Valley Microelectronics, US). In order to develop this device, we used multilayer soft-lithography with SU-8 (Microchem, US) as photoresist. Once the mold was ready we used (Tridecafluoro-1,1,2,2-Tetrahydrooctyl)-1-Trichlorosilane (Sigma-Aldrich, US) to prevent the PDMS (polydimethylsiloxane) polymer from sticking to microstructures; at this point replica molding allowed us to obtain functional devices. The master is exposed to chlorotrimethylsilane (Sigma-Aldrich Co.) vapours for 10 min in order to create an anti-sticking silane layer for PDMS. A 10:1 mixture of PDMS prepolymer and curing agent (Sylgard 184, Dow Corning) is prepared and degassed under vacuum for 1 hour. Then the mixture is poured on the mold, and it is cured on a hot plate at 80°C for 3 hours to facilitate the polymerization and the cross-linking. The PDMS

layer, containing the microfluidic channels, is then peeled from the master and it is cut with a scalpel to separate the single devices; holes are bored through them with a 20-gauge blunt needle in order to create fluidic ports for the access of cells and liquid substances. The PDMS layers obtained are rinsed in isopropyl alcohol in a sonic bath for 10 min to remove debris. For each PDMS piece containing microchannels a thin glass slide (150 μm) is cleaned in acetone and isopropyl alcohol in a sonic bath for 10 min for each step. Finally the PDMS layers and glass slides are exposed to oxygen plasma in a RIE (Reactive Ion Etching) machine for 10 s and brought into contact to form a strong irreversible bond between the two surfaces. As last step all devices were checked for faults inside and outside the channels.

Supplementary Note 5: Doxycycline treatment of PFL and PNFL clones with the microfludics device

PFL and PNFL cells were loaded into the cell traps of the microfluidic device (as described in Materials and Methods) at a seeding density of 10 to 20 cells per trap; the average fluorescence intensity of the cells in at least 3, and up to 20, traps per experiment was tracked by time-lapse microscopy at 15 min intervals, and image analysis was performed as described ([24]). The microfluidics platform enables to change in real-time growth conditions of cells by switching between two different media. We provided the cells with untreated growth medium for two hours, to rule out any fluctuation in metabolism due to displacement of the device from the cell incubator to the incubation chamber of the microscope; we then switched to Doxycycline-treated medium (1 $\mu g/mL$) for different time intervals, according to the simulations: 960 min (Figure 2c in the main text) or 1800 min (Figure 2d in the main text) for PFL cells, and 60 min (Figure 1c in the main text) or 240 min (Figure 1d in the main text) for PNFL cells. After the Doxycycline pulse, cells were switched again to untreated medium for the rest of the experiment. We quantified the mean fluorescence for each group of cells in a trap, as to rule out cell-to-cell variability, and we plotted the mean and standard deviation among all traps (i.e. replicates) for

each experiment.

To transduce cells with the virus produced, 500,000 CHO wild type (in order to obtain PFL and PNFL clones) cells were plated and incubated overnight. On the day of transduction the medium was removed and 1mL of the virus was added to the cells together with polybrene (Invitrogen) to a final concentration of 6ug/mL. After an overnight incubation the medium containing the virus was removed and replaced with complete culture medium containing Blasticidin (Sigma) to a final concentration of 5μg/mL to select for stably transduced cells.

Cells were sorted for fluorescence intensity using a BD FACSAria Cell Sorting System (Becton Dickinson). d2EYFP was excited at 488 nm, and emission was detected using a 525 nm bandpass filter. Serial dilutions of PFL stably transduced cells (up to 0.05 cells/mL) were plated in 96-well microtitre plates, and dilutions containing only one cell per well were selected. Monoclonal colonies were cultured and amplified as described, to obtain monoclonal populations. Monoclonal CHO-PFL cell lines were transduced with the virus carrying the NFL with the same procedure. Cells were sorted for fluorescence intensity using a BD FACSAria Cell Sorting System (Becton Dickinson). mCherry was excited at 587nm, and emission was detected using a 610 nm bandpass filter. Monoclonal population of infected cells were isolated as described above to generate the PNFL cell lines.

Supplementary Note 6: Stochastic analysis of the PFL and PNFL circuits: simplified model

In order to investigate the effect of the miRNA on the protein noise level, we used a simplified model of gene expression as shown in Supplementary Figure S7, where the mRNA is assumed to be transcribed in bursts and proteins are translated from single mRNA molecules [34]. In this simplified model it is possible to derive differential equations describing the time evolution of the different statistical moments of the mRNA and protein counts [34]. We thus derived an analytical expression for the steady-state protein noise level $CV^2 =$ (Squared Coefficient of Variation) as function of the mean number of mRNA

molecules ($\overline{m}$) for the four configurations in Supplementary Figure S7 following the method derived by [34].

Following [34], the Squared Coefficient of Variation CV^2 for a simple transcription-translation model (NOPFL in Supplementary Fig. S7a) can be written as:

$$CV^2{}_{NOPFL} = \frac{\gamma_p(< B > + < B^2 >)}{2 < B > (\gamma_p + \gamma_m) < \overline{m} >}, \tag{S9}$$

where γ_m and γ_p represent the degradation rates for the mRNA and the corresponding protein, B is the number of mRNA molecules produced per burst of transcription, $\overline{m}$ is the mean number of mRNA molecules at the steady state.

In the case of regulated transcription, where the protein activates its own transcription, as depicted in Supplementary Fig. S7b (PFL), the following expression can be derived:

$$CV^2{}_{PFL} = \frac{\gamma_p(< B > + < B^2 >)}{2 < B > (\gamma_p + \gamma_m)(1 - \overline{k}) < \overline{m} >}; \tag{S10}$$

where $\overline{k}$ (a positive number) represents the effect of the protein on the mRNA transcription rate. By comparing Eq.S9 to Eq.S10 it is immediately clear that $CV^2{}_{PFL}$ is always greater than $CV^2{}_{NOPFL}$, that is the PFL increases noise levels.

In order to derive a simplified expression for CV^2 in the presence of a miRNA, we assumed that the miRNA is transcribed together with the mRNA as represented in Supplementary Figure S7c and that the degradation rate of the mRNA is proportional to the number of miRNA molecules, which in turn are proportional to the number of mRNA molecules, thus yielding the following equation for the mRNA degradation rate:

$$\gamma_m(m) = \left(1 - k\frac{m - < \overline{m} >}{< \overline{m} >}\right)\overline{\gamma_m}. \tag{S11}$$

We can now write the following set of differential equations for the Negative Feedback Loop in Supplementary Figure S7c:

$$\frac{d<m>}{dt} = k_m <B> - <\gamma_m m> \tag{S12}$$

$$\frac{d<p>}{dt} = k_p <m> - \gamma_p <m> \tag{S13}$$

$$\frac{d<m^2>}{dt} = k_m <B^2> + 2k_m <B><m> + <\gamma_m(m)m> - 2<\gamma_m(m)m^2> \tag{S14}$$

$$\frac{d<mp>}{dt} = k_m <B><p> - <\gamma_m mp> + k_p <m^2> - \gamma_p <mp> \tag{S15}$$

$$\frac{d<p^2>}{dt} = k_p <m> + 2k_p <mp> + \gamma_p <p> - 2\gamma_p <p^2> \tag{S16}$$

$$\tag{S17}$$

As before, denoting the number of mRNA and protein molecules at steady state by $<\overline{m}>$ and $<\overline{p}>$, we obtain:

$$CV^2{}_{NFL} = \frac{\gamma_p(<B> + <B^2>)}{2<B>(\gamma_p + \gamma_m(1+\overline{\overline{k}}))<\overline{m}>}. \tag{S18}$$

where the parameter $\overline{\overline{k}}$ is a positive real number representing the effect of the miRNA on mRNA degradation.

By comparing Eq.S9, Eq.S10 and Eq.S18, we can check that the following relationship is always satisfied: $CV^2{}_{NFL} \leq CV^2{}_{NOPFL} \leq CV^2{}_{PFL}$. Hence the effect of miRNA acting on mRNA degradation is to decrease noise in protein levels.

The case of a transcriptional PFL coupled to a miRNA-mediated NFL, as shown in Supplementary Figure S7, is less straightforward and it is harder to derive an analytical expression for CV^2, hence we formulated an heuristic approximation for the PNFL by analogy to the previous results:

$$CV^2{}_{PNFL} = \frac{\gamma_p^*(<B> + <B^2>)}{2<B>(\gamma_p^* + \gamma_m^*(1+\overline{\overline{k}}))(1-\overline{k})<\overline{m}>} \tag{S19}$$

The value of $CV^2{}_{PNFL}$ now depends both on the strength of the positive

feedback loop mediated by the protein $\overline{k}$ and on the strength of the negative feedback loop $\overline{\overline{k}}$ mediated by the miRNA.

Figure 4b in the main text shows a graph of the protein noise level (in red) for the PNFL motif (${CV^2}_{PNFL}$) as a function of the mRNA expression level ($\overline{m}$) compared to the protein noise level (in blue) of the PFL motif (${CV^2}_{PFL}$) rescaled and fitted to the experimental data obtained by FACS analysis of the PFL and PNFL clones.

The numerical values of the parameters in Eq.S10 and Eq.S19 used in Figure 4b in the main text were derived as follows: γ_m and γ_p correspond to the parameters d_1 and d_2 in Supplementary Table S1, whereas $< B >$ and $< B^2 >$ were chosen to minimize the Mean Squared Error to the experimental FACS data in Figure 4b. Supplementary Table S2 lists the values of the fitted parameters.

Equations S10 and S19 can be used also to analyze how noise reduction depends on the strength of the PFL. Indeed, the formulas can be generalized using the following functions of the PFL strength ($\overline{k}$):

$$ {CV^2}_{PFL}(\overline{k}) = \frac{A}{1-\overline{k}}, $$

$$ {CV^2}_{PNFL}(\overline{k}) = \frac{B}{1-\overline{k}}, $$

where A and B are constant. It is easy to verify that $A > B$ and this simple relation implies that ${CV^2}_{PFL}(\overline{k}) > {CV^2}_{PNFL}(\overline{k})$ for every value of $\overline{k}$, thus demonstrating that the PFL circuit is always noiser than the PNFL one.

Supplementary Note 7: Stochastic analysis of the PFL and PNFL circuits: detailed model

The advantage of the simplified model, presented in the previous section, is that it allows to compare analytically the CV^2 for the different motifs; the disadvantage is that the model maybe too simplified thus yielding unrealistic results.

We therefore also derived two master equations, one for the PNFL and one for the PFL motif, which take into account the discrete and stochastic nature of chemical reactions [31, 53].

In order to write the PNFL master equation, we generalized the deterministic model described by Eqs.S8-6 and disregarded Eqs.7-10 describing the dynamics of the reporter proteins.

By denoting the tTA mRNA, tTA protein and miR223 mRNA with the variables $w \triangleq x_1$,$q \triangleq x_2$ and $r \triangleq x_4$ and assuming quasi-steady state for Eq.(6) so that $x_3 \propto x_4$, the deterministic model for the PNFL (Eqs.S8-4) becomes:

$$\frac{dw}{dt} = (\overline{K_w} + K_w(q)) - g_w w - \beta_w(r) w \tag{S20}$$

$$\frac{dq}{dt} = K_q w - g_q q \tag{S21}$$

$$\frac{dr}{dt} = (\overline{K_r} + K_r(q)) - g_r r \tag{S22}$$

where $\overline{K_w} = G_1 v_1 \alpha_1$, $K_w(q) = G_1 v_1 (1-\alpha_1) \frac{q^{h_2}}{K_1^{h_2} + q^{h_2}}$, $g_w = d_1$, $\beta_w(r) = \lambda \frac{r^{h_3}}{{K_3}^{h_3} + r^{h_3}}$, $K_q = v_2$, $g_q = d_2$, $\overline{K_r} = G_2 v_1 \alpha_1$ and $K_r(q) = K_w(q)$.

Similarly, the PFL model in [24] can be rewritten as:

$$\frac{dw}{dt} = (\overline{K_w} + K_w(q)) - g_w w \tag{S23}$$

$$\frac{dq}{dt} = K_q w - g_q q \tag{S24}$$

Following the method described in [31], we linearized the nonlinear functions $K_w(q)$, $K_r(q)$ and $\beta_w(r)$ to obtain:

$$K_w(q) \simeq {K_w}^0 + {K_w}^1 q \tag{S25}$$

$$K_r(q) \simeq {K_r}^0 + {K_r}^1 q \tag{S26}$$

$$\beta_w(r) \simeq {\beta_w}^0 + {\beta_w}^1 r \tag{S27}$$

where ${K_w}^0$,${K_w}^1$,${K_r}^0$,${K_r}^1$,${\beta_w}^0$ and ${\beta_w}^1$ are constant terms.

The Master equation for the PFL circuit can be derived as:

$$\frac{\partial P_{w,q}}{\partial t} = (\overline{K_w} + K_w(q))(P_{w-1,q} - Pw, q) + \\ K_q w(P_{w,q-1} - Pw, q) + g_w((w+1)P_{w+1,q} - wP_{w,q}) \\ + g_q((q+1)P_{w,q+1} - qP_{w,q}) \tag{S28}$$

Introducing the moment generating function,([31, 53]):

$$F(z_1, z_2) = \sum_{w,q} {z_1}^w {z_2}^q P_{w,q}, \tag{S29}$$

it is possible to derive the following Partial Differential Equation (PDE) equation:

$$\partial_t F = (\overline{K_w} + {K_w}^0)F(z_1 - 1) + \\ + {K_w}^1 z_2 \partial_{z_2} F(z_1 - 1) + \\ + K_q z_1 \partial_{z_1} F(z_2 - 1) + \\ + g_w \partial_{z_1} F(1 - z_1) + g_q \partial_{z_2} F(1 - z_2) \tag{S30}$$

which at the steady state becomes:

$$(\overline{K_w} + {K_w}^0)F(z_1 - 1) + {K_w}^1 z_2 \partial_{z_2} F(z_1 - 1) + \\ + K_q z_1 \partial_{z_1} F(z_2 - 1) + g_w \partial_{z_1} F(1 - z_1) + g_q \partial_{z_2} F(1 - z_2) = 0 \tag{S31}$$

From this equation, we can estimate the moments of the distribution in order to evaluate the $CV = \frac{\sigma_q}{<q>} = \frac{\sqrt{F_{22} - {F_2}^2 + F_2}}{F_2}$.

The moments are listed below:

$$F_1 = \frac{g_q(\overline{K_w} + {K_w}^0)}{(g_w g_q - {K_w}^1 K_q)} \tag{S32}$$

$$F_2 = \frac{K_q F_1}{g_q} \tag{S33}$$

$$F_{12} = \frac{g_q F_2[(\overline{K_w} + {K_w}^0 + {K_w}^1)g_w + g_q g_w + (\overline{K_w} + {K_w}^0)g_q]}{(g_w + g_q)(g_w g_q - {K_w}^1 K_q)} \tag{S34}$$

$$F_{11} = \frac{(\overline{K_w} + {K_w}^0)F_1 + {K_w}^1 F_{21}}{g_w} \tag{S35}$$

$$F_{22} = \frac{K_q F_{12}}{g_q} \tag{S36}$$

where it is possible to demonstrate that F_{12} equals F_{21}.

Similarly, we derived **the Master Equation for the PNFL circuit**:

$$\begin{aligned}
\frac{\partial P_{w,q,r}}{\partial t} &= (\overline{K_w} + K_w(q))(P_{w-1,q,r} - P_{w,q,r}) + \\
&+ K_q w(P_{w,q-1,r} - P_{w,q,r}) + \\
&+ (\overline{K_w} + K_w(q))(P_{w,q,r-1} - P_{w,q,r}) + \\
&+ g_w((w+1)P_{w+1,q,r} - wP_{w,q,r}) + \\
&+ g_q((q+1)P_{w,q+1,r} - qP_{w,q,r}) + \\
&+ g_r((r+1)P_{w,q,r+1} - rP_{w,q,r}) + \\
&+ \beta_w(r)((w+1)P_{w+1,q,r} - wP_{w,q,r})
\end{aligned} \tag{S37}$$

Using the moment generating function:

$$F(z_1, z_2, z_3) = \sum_{w,q,r} {z_1}^w {z_2}^q {z_3}^r P_{w,q,r} \tag{S38}$$

it is possible to derive a PDE equation:

$$\begin{aligned}\partial F_t = &(\overline{K_w} + {K_w}^0)(z_1 - 1)F + \\ &+ {K_w}^1 z_2 F_1(z_1 - 1) + K_q z_1 F_1(z_2 - 1) + \\ &+ (\overline{K_w} + {K_w}^0)F(z_3 - 1) + {K_w}^1 z_2 F_2(z_3 - 1) + \\ &+ g_w F_1(1 - z_1) + g_q F_2(1 - z_2) + g_r F_3(1 - z_3) + \\ &+ {\beta_w}^0 F_1(1 - z_1) + {\beta_w}^1 z_3 F_{13}(1 - z_1)\end{aligned} \tag{S39}$$

which at the steady state becomes:

$$\begin{aligned}&(\overline{K_w} + {K_w}^0)(z_1 - 1)F + {K_w}^1 z_2 F_1(z_1 - 1) + K_q z_1 F_1(z_2 - 1) + \\ &+ (\overline{K_w} + {K_w}^0)F(z_3 - 1) + {K_w}^1 z_2 F_2(z_3 - 1) + g_w F_1(1 - z_1) + \\ &+ g_q F_2(1 - z_2) + g_r F_3(1 - z_3) + {\beta_w}^0 F_1(1 - z_1) + \\ &+ {\beta_w}^1 z_3 F_{13}(1 - z_1) = 0\end{aligned} \tag{S40}$$

From this equation, it is possible to estimate the moments in order to evaluate the $CV = \frac{\sigma_q}{<q>} = \frac{\sqrt{F_{22} - {F_2}^2 + F_2}}{F_2}$:

$$F_1 = \frac{(\overline{K_w} + {K_w}^0 - {\beta_w}^0) + {K_w}^1 F_2 - {\beta_w}^1 F_3}{g_w} \tag{S41}$$

$$F_2 = \frac{K_q F_1}{g_q} \tag{S42}$$

$$F_3 = \frac{(\overline{K_r} + {K_r}^0) + {K_r}^1 F_2}{g_r} \tag{S43}$$

$$F_{11} = \frac{(\overline{K_w} + {K_w}^0 - {\beta_w}^0) F_1 + {\beta_w}^1 (F_3 - F_{31}) + {K_w}^1 F_{21} + {\beta_w}^0}{g_w} \tag{S44}$$

$$F_{12} = \frac{(\overline{K_w} + {K_w}^0 + {K_w}^1 - {\beta_w}^0) F_2 + {K_w}^1 F_{22} + K_q F_{11}}{g_w + g_q} + \\ + \frac{K_q F_1 - {\beta_w}^1 F_{32}}{g_w + g_q} \tag{S45}$$

$$F_{13} = \frac{(\overline{K_w} + {K_w}^0 - {\beta_w}^0 - {\beta_w}^1) F_3 + (\overline{K_r} + {K_r}^0) F_1}{g_w + g_r} + \\ + \frac{{K_r}^1 F_{21} + {K_w}^1 F_{23} - {\beta_w}^1 F_{33}}{g_w + g_r} \tag{S46}$$

$$F_{22} = \frac{K_q F_{12}}{g_q} \tag{S47}$$

$$F_{23} = \frac{(\overline{K_r} + {K_r}^0 - {K_r}^1) F_2 + {K_r}^1 F_{22} + K_q F_{13}}{g_r + g_q} \tag{S48}$$

$$F_{33} = \frac{(\overline{K_r} + {K_r}^0) F_3 + {K_r}^1 F_{23}}{g_r} \tag{S49}$$

We numerically solved Eqs. (S32 - S36) for the PFL and Eqs.(S41 - S49) for the PFL to simulate the CV^2 as function of the mean protein level. Results are shown in Supplementary Figure S8 and parameters used for the simulations are reported in Supplementary Table S3. This analysis further confirms our thesis of an higher robustness of the PNFL circuit compared to the PFL in terms of protein noise levels. In the same Supplementary Figure S8 the simulation for the NOPFL is also reported using the moments already computed in [31] for the open circuit (TF - target) in which the parameters in common to our PFL were chosen with the same values.

Supplementary Note 8: Treatment of PNFL cells with miR223 LNA

PFNL 7.2 cells were pre-treated with 1 μg /ml Doxycycline for 72 hrs. After Doxycycline removal, cells were plated in a 12-well culture plate at different densities thus obtaining 400.000 cells per well for each collecting time point. The cells were transfected 24 hrs after seeding with 150 pmol of Locked Nucleic Acid (EXIQON)223 and with a scramble using Lipofectamine 2000, (Life technologies) according to manufacturer's instructions . Fluorescence was measured by FACS analysis at 0, 24, 48, 72 and 96 hrs after Doxycycline removal. Each FACS measurement was made on a sample of 20.000 events in duplicate.

Supplementary Note 9: Image acquisition and processing

Image acquisition was performed using a Nikon Eclipse TI-E inverted epifluorescence microscope, equipped with a digital camera (Andor Clara, Andor) and an incubation chamber (H201-OP R2, Okolab), a PlanFluor 40x Ph2 DLL objective, a TRITC filter (excitation 530/30 nm, emission 590nm/ 60nm, Nikon) and a FITC filter (excitation 460/40 nm, emission 510nm/ 50nm, Nikon). Exposure time was set to 30 ms for the bright field images (with transmitted light lamp voltage was set to 3V), 300 ms for observation of d2EYFP, and 700 ms for observation of Sulphorhodamine tracker. Temperature was maintained constantly at 37°C, and CO2 concentration was set to 5% of the total air volume injected in the incubation chamber. Experiments were performed and images were extracted using the NIS-Elements AR v.3.22.14 software package and the Perfect Focus System (Nikon Instruments) to maintain the focal plane throughout the experiment.

Supplementary References

[51] Cuccato, G. *et al.* Modeling RNA interference in mammalian cells. BMC *Systems Biology* 5, 1-9 (2011).

[52] Bogacki, P. & Shampine, L. F. A 3(2) pair of Runge-Kutta formulas. *Appl. Numer. Math.* 2, 1-9 (1989).

[53] Thattai, M. & van Oudenaarden, A. Intrinsic noise in gene regulatory networks. *Proceedings of the National Academy of Sciences* 98, 8614-8619 (2001).
[54] Tigges, M., Marquez-Lago, T. T., Stelling, J. & Fussenegger, M. A tunable synthetic mammalian oscillator. *Nature* 457, 309-312 (2009).